THE JOURNAL OF PHYSICAL CHEMISTRY A
A JOURNAL OF THE AMERICAN CHEMICAL SOCIETY

pubs.acs.org/JPCA

Article

Carbon Condensation *via* [4 + 2] Cycloaddition of Highly Unsaturated Carbon Chains

Andrew N. Owen, Brian J. Esselman, R. Claude Woods, and Robert J. McMahon*

Cite This: *J. Phys. Chem. A* 2023, 127, 4277−4290

Read Online

ACCESS | Metrics & More | Article Recommendations | Supporting Information

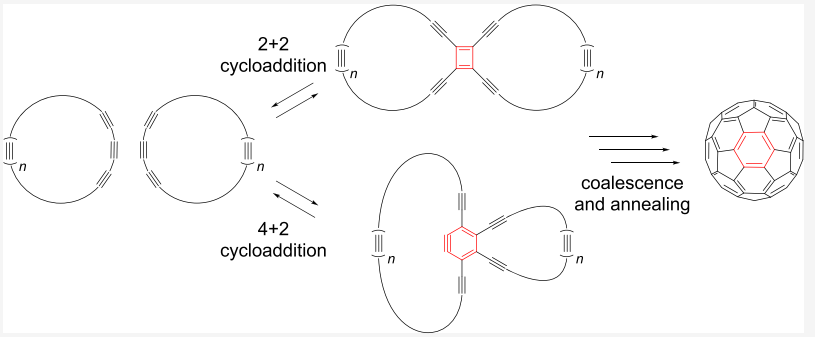

ABSTRACT: We present computational studies of reaction pathways for alkyne/polyyne dimerization that represent plausible early steps in mechanisms for carbon condensation. A previous computational study of the ring coalescence and annealing model of C_{60} formation revealed that a 1,4-didehydrobenzocyclobutadiene intermediate (*p*-benzyne derivative) has little to no barrier to undergoing an unproductive retro-Bergman cyclization, which brings into question the relevance of that reaction pathway. The current study investigates an alternative model, which proceeds through an initial [4 + 2] cycloaddition instead of a [2 + 2] cycloaddition. In this pathway, the problematic intermediate is avoided, with the reaction proceeding *via* a (potentially) more kinetically stable tetradehydronaphthalene derivative. The computational studies of the [2 + 2] and [4 + 2] model systems, with increasing alkyne substitutions, reveal that the *para*-benzyne diradical of the [4 + 2] pathway has a significantly greater barrier to ring opening than the analogous intermediates of the [2 + 2] pathway and that alkyne substitution has little effect on this important barrier. These studies employ spin-flip, time-dependent density functional theory (SF-TDDFT) to provide suitable treatment of open-shell diradical intermediates.

INTRODUCTION

Allotropes of carbon continue to be active areas of research in chemistry and materials science. Recent studies include a monolayer fullerene network,[1] graphene nanoribbons of various geometries,[2] and allotropes derived from nonbenzenoid aromatic structures (azulene, biphenylene, *etc.*).[3] Cyclocarbon C_{18},[4,5] a known precursor of C_{60},[6] has been imaged on a surface.[7] A myriad of chemical models for the formation of fullerene have been proposed and can be categorized into two groups: pathways that start from large carbon aggregates that degrade into fullerene ("size-down") and pathways that start from small carbon aggregates and condense into fullerene ("size-up"). The "size-down" pathways that have been proposed include the degradations of graphene,[8,9] graphene nanoflakes,[10] carbon nanotubes,[11] and giant fullerenes.[12,13] The "size-up" pathways proposed include the fullerene road,[14] pentagon road,[15] closed network growth,[15−17] and ring coalescence and annealing.[6,18,19] All of the "size-up" pathways except the ring coalescence and annealing model progress from smaller carbon aggregates to larger fullerenes through the steady incorporation of C_2 fragments. In contrast, the ring coalescence and annealing model proposes the addition of medium-sized (C_{12}−C_{20}) cyclic polyynes, and subsequent annealing through a cascading radical mechanism, resulting in fullerenes.[20] As illustrated in Scheme 1, this combination has been proposed to occur through an initial [2 + 2] cycloaddition to yield a tetraalkynylcylcobuta-1,3-diene intermediate that subsequently undergoes a Bergman cyclization reaction.[19,20] While formation of a tetraalkynylcyclobutadiene may be a reasonable step in this process, it was previously shown[21] that the model products formed by the subsequent Bergman cyclization reaction may have little or no barrier to undergo an exothermic ring expansion (*via* a retro-Bergman cyclization mechanism) to yield an eight-membered ring

Received: January 27, 2023
Revised: April 14, 2023
Accepted: April 18, 2023
Published: May 5, 2023

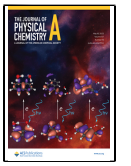

https://doi.org/10.1021/acs.jpca.3c00617
J. Phys. Chem. A 2023, 127, 4277−4290

Scheme 1. [2 + 2] Ring Coalescence and Annealing Model of Fullerene Formation

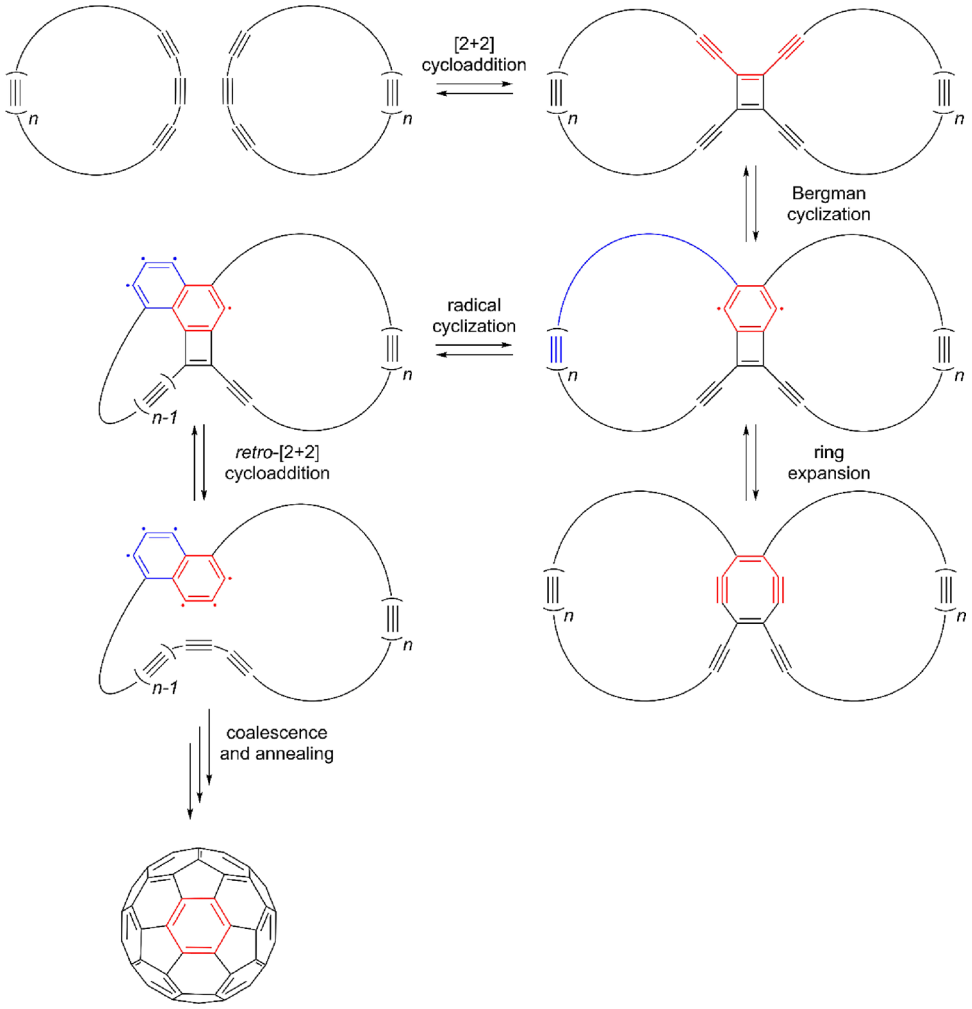

intermediate. This eight-membered ring intermediate is not currently accounted for in the ring coalescence and annealing model, and the structural element of an eight-membered ring is obviously not present in fullerene C_{60}. These findings call into question whether or not the initial [2 + 2] dimerization represents a productive pathway to fullerene formation. With this in mind, we turned our attention to the study of an alternative reaction pathway that involves initial [4 + 2] cycloaddition, or hexadehydro-Diels-Alder reaction (HDDA),[22,23] of two polyynes to give a tetraalkynyl *ortho*-benzyne intermediate (Scheme 2). Subsequent Bergman cyclization—followed by a cascading radical mechanism—may afford a viable pathway to C_{60}, as illustrated in Scheme 2. This pathway avoids forming a high-energy, four-membered ring intermediate and avoids the problematic ring expansion leading to the eight-membered ring species. In this study, we investigate whether a small modification to the ring coalescence and annealing model yields a more kinetically realistic reaction pathway.

The condensation of highly unsaturated carbon molecules *via* cycloaddition reactions has been evaluated computationally at several levels of theory for a variety of species, as summarized in Scheme 3, but the comparison of polyyne dimerization through [2 + 2] or [4 + 2] cycloaddition reactions has not been made. A thermal, concerted $[2\pi_s + 2\pi_s]$ cycloaddition is symmetry forbidden, and the [2 + 2] cycloaddition is expected to proceed through a radical mechanism (top Scheme 3).[24−26] The [4 + 2] cycloaddition can proceed through either a radical mechanism or a concerted $[4\pi_s + 2\pi_s]$ mechanism, with the concerted reaction having an activation barrier of 34−36 kcal/mol, compared to the rate-determining step of the radical mechanism having a barrier of 30−37 kcal/mol (middle Scheme 3).[26−28] The competition of the [2 + 2] cycloaddition versus the [4 + 2] cycloaddition is exemplified by the combination of butadiyne and acetylene (middle Scheme 3, gray and underlined) to form either *ortho*-benzyne or ethynylcyclobutadiene.[26] The computed barriers for stepwise and concerted processes are close in energy, and the overall prediction of stepwise vs concerted depends on the level of theory employed. Overall, the formation of the [4 + 2] product (*ortho*-benzyne) is significantly more exothermic (>40 kcal/mol) than the formation of the [2 + 2] product (ethynylcyclobutadiene).[26] It is worth noting that in the stepwise pathway for the reaction of *ortho*-benzyne and butadiyne (bottom Scheme 3), the [2 + 2] product is kinetically favored by several kcal/mol, while the formation of the [4 + 2] product is thermodynamically favored by about 30 kcal/mol.[25]

Following initial cycloadditions of the polyynes, the next step toward fullerene formation in the ring coalescence and annealing model is a Bergman cyclization.[20,29] The resulting intermediate for the [2 + 2] pathway is a substituted

https://doi.org/10.1021/acs.jpca.3c00617
J. Phys. Chem. A 2023, 127, 4277−4290

Scheme 2. Proposed [4 + 2] Ring Coalescence and Annealing Model of Fullerene Formation

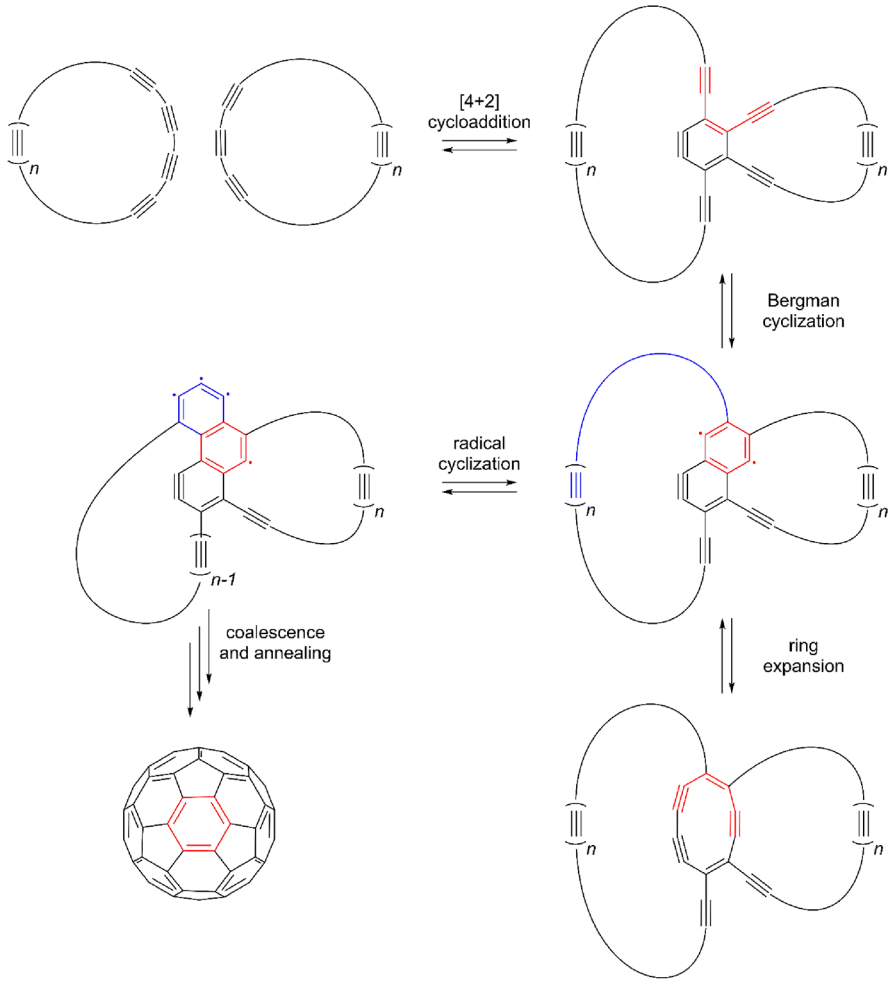

tetraalkynyl-didehydrobenzocyclobutadiene, which is a fused *para*-benzyne and cyclobutadiene species (Scheme 1). The resulting intermediate for the [4 + 2] pathway is a substituted tetraalkynyl-tetradehydronaphthalene, which is a fused *ortho*- and *para*-benzyne species (Scheme 2). In principle, the *para*-benzyne intermediate of the [4 + 2] pathway is expected to be more stable than the corresponding *para*-benzyne intermediate of the [2 + 2] pathway; the *ortho*-benzyne present in the former is a strained, formally aromatic ring while the cyclobutadiene present in the latter is a more highly strained, formally antiaromatic ring. This argument is supported by the computational result that the [4 + 2] product of *ortho*-benzyne and butadiyne is 30 kcal/mol lower in energy than the [2 + 2] product (bottom Scheme 3). With the [4 + 2] intermediate considerably lower in energy than the [2 + 2] intermediate, the subsequent ring expansion (*via* a retro-Bergman cyclization mechanism) will have a greater barrier within the [4 + 2] pathway than within the [2 + 2] pathway. The [4 + 2] pathway would thus be more likely to undergo the subsequent cascading radical mechanism that leads to fullerene production.

The [2 + 2] and [4 + 2] carbon condensation pathways (**I** and **II**, respectively) studied in this work are illustrated in Scheme 4. Because computational studies of large carbon ring systems, as described in Schemes 1 and 2, are not computationally feasible with reasonable *ab initio* methods, we used a simplified substitution pattern described in Scheme 4 (**a**–**d**). Substitution **a** is the parent system (R = R′ = H). Substitution **b** places additional alkynyl units at the end of the alkyne chains of the cycloaddition products **2b** or **6b**, while substitution **c** places additional alkynyl units on the ring of the cycloaddition products **2c** or **6c**. The **d** substitution places alkynyl units on both the ring and the alkyne chains of the cycloaddition products **2d** or **6d**. Scheme 4 (top) illustrates a [2 + 2] cycloaddition pathway involving two polyynes (**1a**–**d**) to yield substituted cyclobutadiene **2a**–**d**. A Bergman cyclization of the enediyne unit of **2a**–**d** results in the diradical didehydrobenzocyclobutadiene **3a**–**d**. Diradical species **3a**–**d** can then undergo the ring expansion, breaking the shared carbon–carbon bond between the fused rings, to generate cycloocta-1,5-dien-3,7-diyne **4a**–**d**. Scheme 4 (bottom) illustrates an alternative pathway that proceeds through an initial [4 + 2] cycloaddition of two polyynes **1**/**5a**–**d**. Necessarily, the pathway involves an extra alkynyl unit in one of the initial polyynes for system **II** compared to system **I**. The [4 + 2] cycloaddition yields the substituted *ortho*-benzyne **6a**–**d**, which can undergo the Bergman cyclization to generate the diradical tetradehydronaphthalene species **7a**–**d**. The ring expansion of **7a**–**d** generates cyclodeca-1,7-dien-3,5,9-triyne **8a**–**d**. Regardless of whether the initial [2 + 2] or [4 + 2] adducts are formed by a stepwise or concerted process, we are keenly interested in elucidating the chemistry of these enediynes (**2a**–**d** and **6a**–**d**) with respect to Bergman cyclization and subsequent ring opening.

https://doi.org/10.1021/acs.jpca.3c00617
J. Phys. Chem. A 2023, 127, 4277–4290

Scheme 3. Mechanisms of Simple Alkyne Cycloadditions (Relative Energies in kcal/mol)

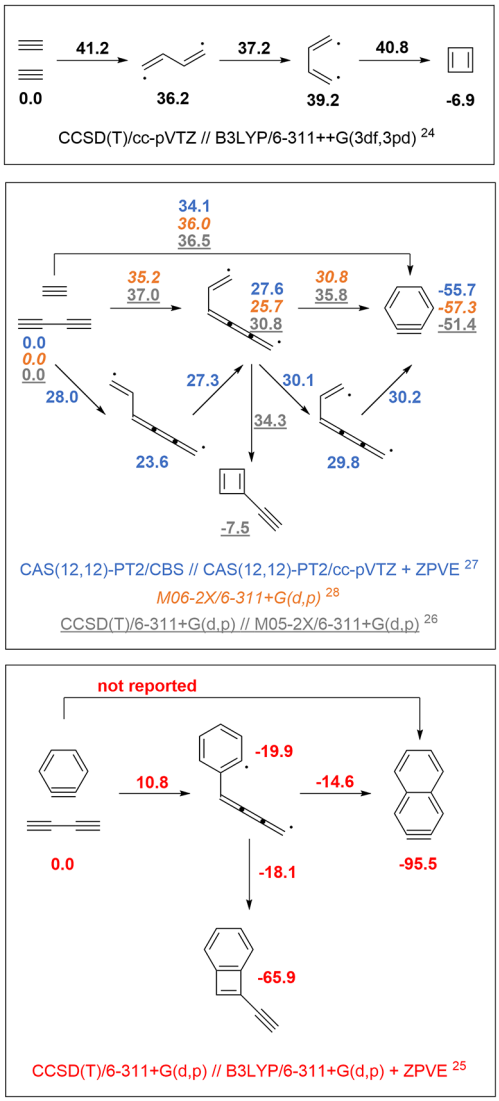

An earlier study of reaction pathway **Ia** using density functional theory (DFT) with the B3LYP functional was unsuccessful at identifying **3a** as a stationary point for the reactions under investigation.[21] Preliminary optimizations of the structures of **3a−d** and **7a−d** using DFT had similar issues and were unsuccessful for functionals including B3LYP, PBE0, PBE50, M06, M06-2X, and ωB97XD as well as for spin-flip DFT functionals including (non)collinear 50-50 and PBE50. To optimize the structures of interest, we used the *ab initio* Møller−Plesset second-order perturbation theory (MP2). The MP2 method successfully optimized all the structures represented in Scheme 4, but—as noted previously[21] and discussed further in this work—the MP2 description of the electronic structure of the diradicals **3a−d** and **7a−d** is questionable. This is because MP2 employs a single-reference model for a species that is best treated with a multireference model. The sizes of the structures in Scheme 4, however, are much too large to be optimized at such a sophisticated and computationally intensive level of theory.

In this work, we revisited pathway **Ia** by utilizing a smaller step size in the intrinsic reaction coordinate (IRC) calculation to increase the sampling and produce a finer-detailed potential energy surface for the purpose of comparison to the spin-flip model system. The multireference equation-of-motion and spin-flip coupled cluster method (EOM-SF-CCSD) employed previously on MP2 single point calculations[21] is computationally too intensive and not suitable for studying the larger systems in this work. Analogous spin-flip approaches have been applied to density functional theory[30] and recent advances in the implementation[31] give comparable results. The spin-flip, time-dependent DFT calculations are less computationally intensive than their coupled-cluster counterparts and can be used to evaluate the energetics of all the reaction pathways in this investigation.

COMPUTATIONAL METHODS

To evaluate the reactions of interest, restricted Møller−Plesset second-order perturbation theory[32] was employed with the correlation-consistent polarized valence and triple-zeta basis set[33] (MP2/cc-pVTZ) using Gaussian 09.[34] Geometry optimizations with harmonic frequency calculations were employed to determine the nature of the stationary points. Intrinsic reaction coordinate (IRC) calculations were used to confirm that each transition state structure smoothly connects the corresponding pair of local minima for all model schemes.

Scheme 4. [2 + 2] and [4 + 2] Reaction Pathways

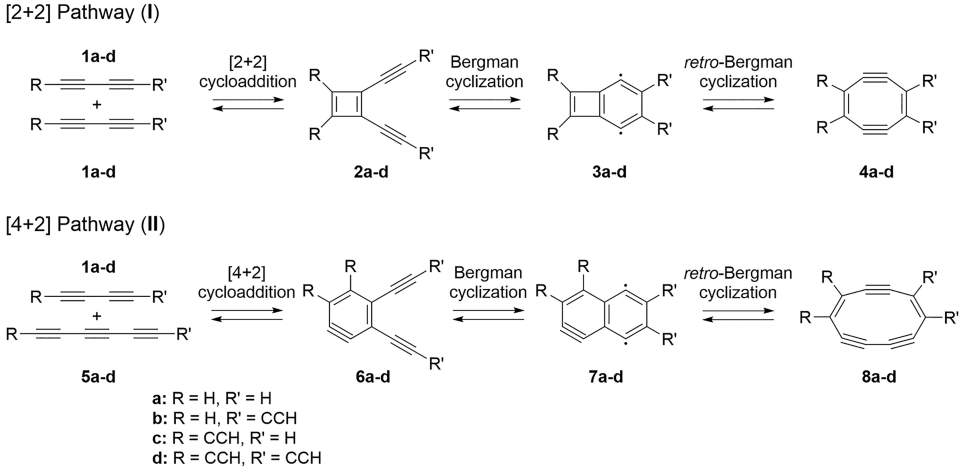

https://doi.org/10.1021/acs.jpca.3c00617
J. Phys. Chem. A 2023, 127, 4277−4290

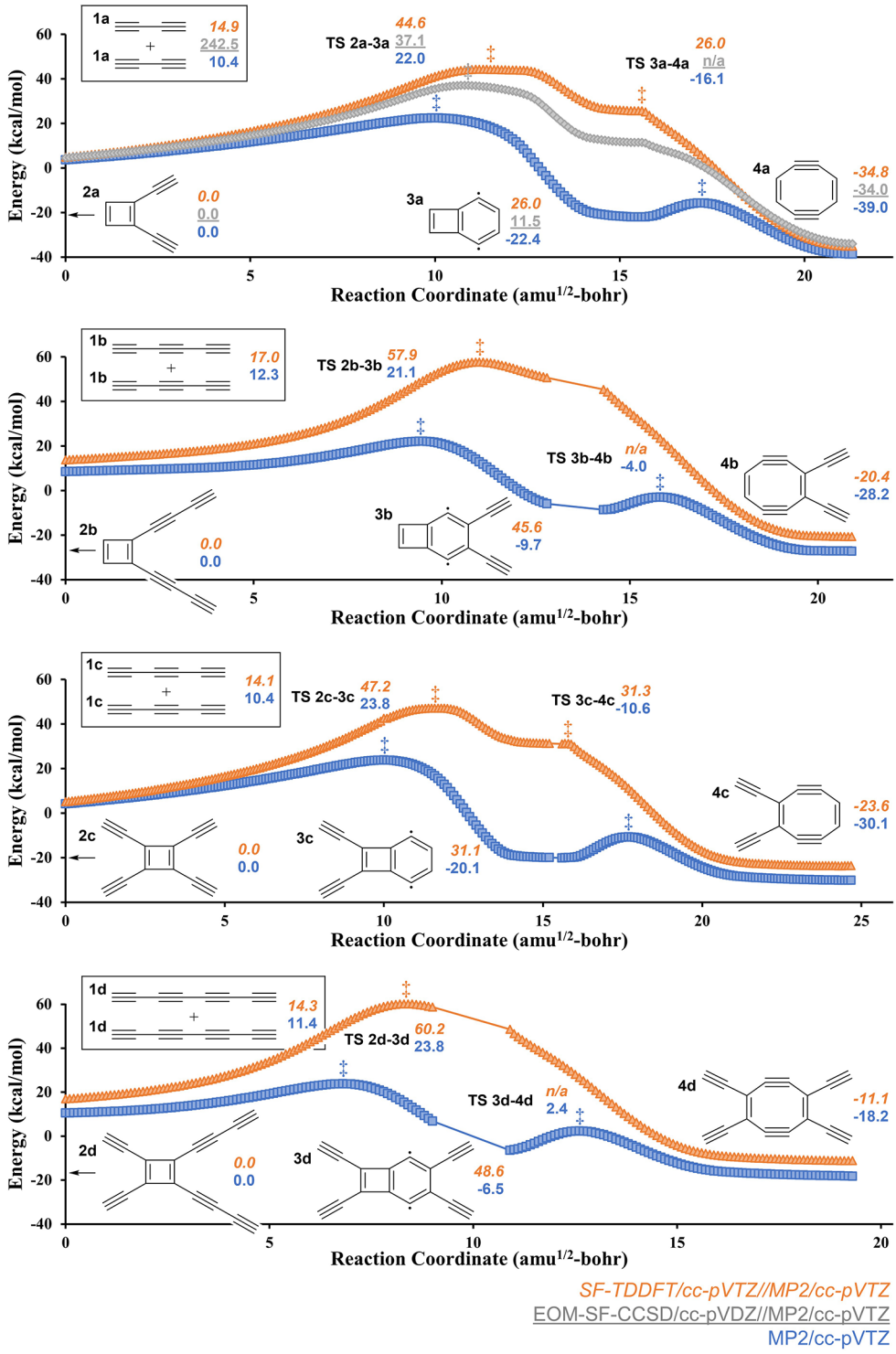

Figure 1. Potential energy surfaces for the Bergman cyclization and ring expansion of alkynyl-substituted cyclobutadienes (system **I**). Straight lines are used to connect the ends of the IRC calculations to their corresponding local minima and are not representative of the true nature of the energy surface. The *x*-axis origin corresponds to the end of the IRC calculation going from **TS 2−3** toward **2**. The local minima of **2a−d** are not shown.

For **Ia** and **IIa**, single point calculations on the MP2 structures were carried out with coupled-cluster calculations (CCSD(T)/cc-pVTZ) and equation-of-motion spin-flip coupled cluster with single and double excitations (EOM-SF-CCSD/cc-pVDZ) as implemented in Q-Chem 4.4.1.[35] For all reaction schemes (**Ia−d** and **IIa−d**), single point calculations on the MP2 structures were carried out using spin-flip time-dependent density functional theory within the Tamm−Dancoff approximation (SF-TDDFT)[30] as implemented in Q-Chem 4.4.1[35] with the cc-pVTZ basis set and utilizing the "collinear 50-50" functional[30] (exchange = 50% HF + 8% Slater + 42% Becke; correlation = 19% VWN + 81% LYP). Additional properties of the MP2/cc-pVTZ local minima were analyzed by nuclear-independent chemical shifts (NICS),[36] using the

https://doi.org/10.1021/acs.jpca.3c00617
J. Phys. Chem. A 2023, 127, 4277−4290

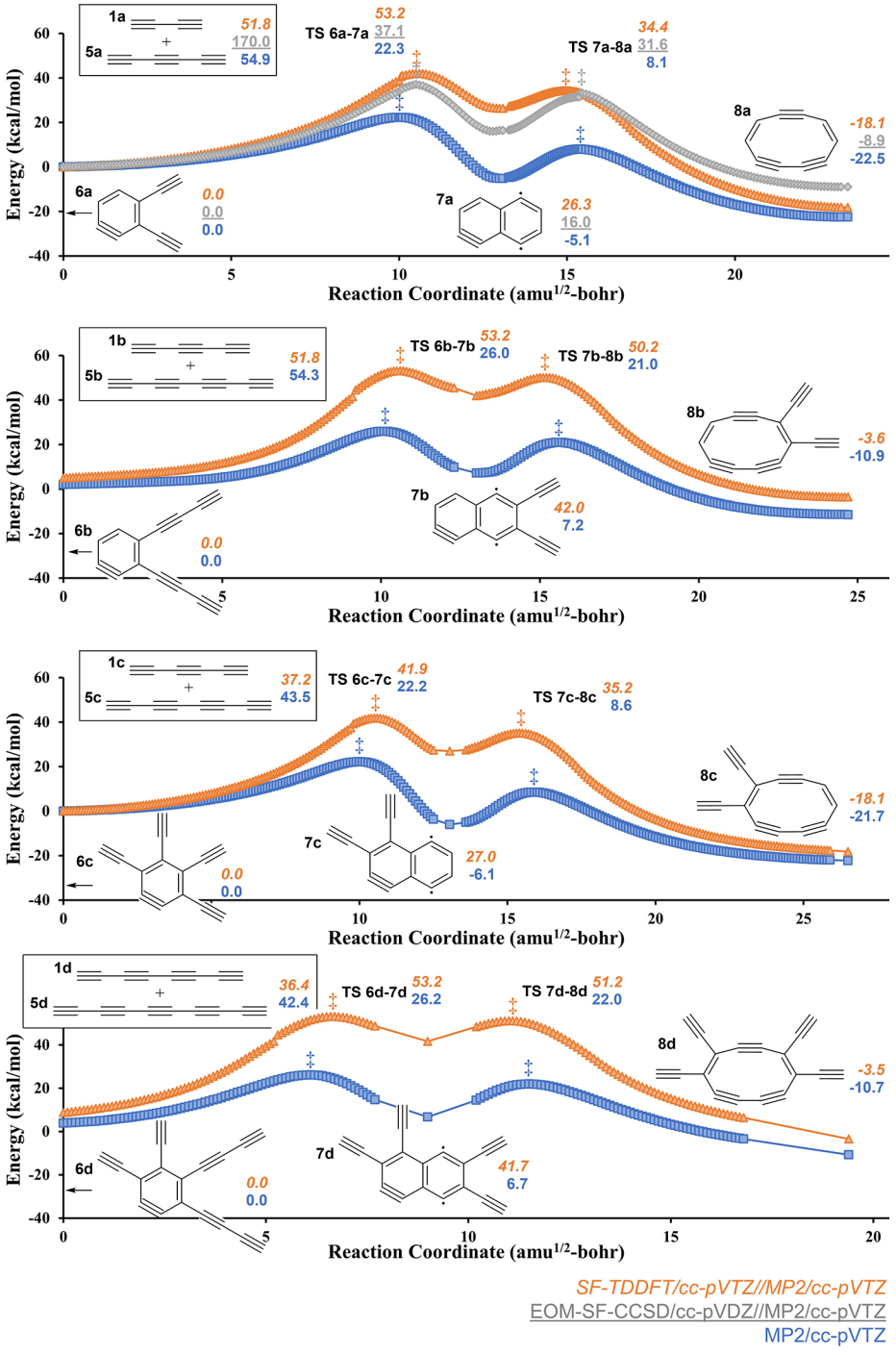

Figure 2. Potential energy surfaces for the Bergman cyclization and subsequent ring expansion of alkynyl-substituted *ortho*-benzynes (system **II**). Straight lines are used to connect the ends of the IRC calculations to their corresponding local minima and are not representative of the true nature of the energy surface. The *x*-axis origin corresponds to the end of the IRC calculation going from **TS 6−7** toward **6**. The local minima of **6a−d** are not shown.

gauge-independent atomic orbital (GIAO) method, and natural bond orbital/natural resonance theory (NBO/NRT)[37] calculations with the B3LYP functional[38,39] and the 6-31G(d) basis set,[40] as implemented in Gaussian 09.[34]

While conducting the EOM-SF-CCSD and SF-TDDFT single-point calculations on the MP2 IRC structures, multiple solutions to the reference SCF calculations were observed for closely related structures. The structures around **3a−d** and **7a−d** resulted in a variety of spin-flip excited states regardless of which reaction pathway or substitution pattern was considered. This is partially explained by considering that, for the high-spin triplet reference, there is a change in the energetic ordering of two non-interacting triplet states that occurs near **TS2−3** and **TS6−7** in almost all substitution patterns (**a−d**). Unfortunately, the reordering of the triplet states does not account for the varied results in the region

https://doi.org/10.1021/acs.jpca.3c00617
J. Phys. Chem. A 2023, 127, 4277−4290

Table 1. Relative Energies (kcal/mol) of Stationary Points

	SF-TDDFT[a]							MP2[d]						
I	**1**[b]	**TS1−2**	**2**[b]	**TS2−3**[c]	**3**[c]	**TS3−4**[c]	**4**[c]	**1**	**TS1−2**	**2**	**TS2−3**	**3**	**TS3−4**	**4**
a	14.9		0.0	44.6	26.0	26.0	−34.8	10.4		0.0	22.0	−22.4	−16.1	−39.0
	[242]		[0.0]	[37.1]	[11.5]	[-]	[−34.0]							
b	17.0		0.0	57.9	45.6		−20.4	12.3		0.0	21.1	−9.7	−4.0	−28.2
c	14.1		0.0	47.2	31.1	31.3	−23.6	10.4		0.0	23.8	−20.1	−10.6	−30.1
d	14.3		0.0	60.2	48.6		−11.1	11.4		0.0	23.8	−6.5	2.4	−18.2
II	**1/5**[b]	**TS1/5−6**[b]	**6**[b]	**TS6−7**[c]	**7**[c]	**TS7−8**[c]	**8**[c]	**1/5**	**TS1/5−6**	**6**	**TS6−7**	**7**	**TS7−8**	**8**
a	51.8	104.7	0.0	42.1	26.3	34.4	−18.1	54.9	83.8	0.0	22.3	−5.1	8.1	−22.5
	[170]	[119]	[0.0]	[37.1]	[16.0]	[31.6]	[−8.9]							
b	51.8		0.0	53.2	42.0	50.2	−3.6	54.3		0.0	26.0	7.2	21.0	−10.9
c	37.2	89.4	0.0	41.9	27.0	35.2	−18.1	43.5	73.8	0.0	22.2	−6.1	8.6	−21.7
d	36.4		0.0	53.2	41.7	51.2	−3.5	42.4	-	0.0	26.2	6.7	22.0	−10.7

[a]Energies calculated at SF-TDDFT/cc-pVTZ//MP2/cc-pVTZ; energies in brackets calculated at EOM-SF-CCSD/cc-pVDZ//MP2/cc-pVTZ. [b]Determined using structures that were stationary points at MP2/cc-pVTZ. [c]Determined using the SF energies to identify stationary points based on PES curvature. [d]Energies calculated at MP2/cc-pVTZ.

Table 2. Energetics (kcal/mol) of Reactions in Systems I and II

	SF-TDDFT[a]						MP2[d]					
	initial cycloaddition (**1−2** and **1/5−6**)		Bergman cyclization (**2−3** and **6−7**)		ring expansion (**3−4** and **7−8**)		initial cycloaddition (**1−2** and **1/5−6**)		Bergman cyclization (**2−3** and **6−7**)		ring expansion (**3−4** and **7−8**)	
	$\Delta E^{\ddagger}$ [b]	ΔE_{rxn} [b]	$\Delta E^{\ddagger}$ [c]	ΔE_{rxn} [c]	$\Delta E^{\ddagger}$ [c]	ΔE_{rxn} [c]	$\Delta E^{\ddagger}$	ΔE_{rxn}	$\Delta E^{\ddagger}$	ΔE_{rxn}	$\Delta E^{\ddagger}$	ΔE_{rxn}
Ia		−14.9	44.6	26.0	0.0	−60.8		−10.4	22.0	−22.4	6.3	−16.6
		[−242]	[37.1]	[11.5]		[−45.4]						
Ib		−17.0	57.9	45.6		−66.0		−12.3	21.1	−9.7	5.7	−18.6
Ic		−14.1	47.2	31.1	0.1	−54.8		−10.4	23.8	−20.1	9.5	−10.0
Id		−14.3	60.2	48.6		−59.8		−11.4	23.8	−6.5	8.9	−11.7
IIa	52.9	−51.8	42.1	26.3	8.1	−44.4	28.9	−54.9	22.3	−5.1	13.2	−17.4
	[−51]	[−170]	[37.1]	[16.0]	[15.6]	[−24.9]						
IIb		−51.8	53.2	42.0	8.2	−45.6		−54.3	26.0	7.2	13.8	−18.7
IIc	52.2	−37.2	41.9	27.0	8.2	−45.1	30.3	−43.5	22.2	−6.1	14.6	−16.2
IId		−36.4	53.2	41.7	9.5	−45.1		−42.4	26.2	6.7	15.3	−17.5

[a]Energies calculated at SF-TDDFT/cc-pVTZ//MP2/cc-pVTZ; energies in brackets calculated at EOM-SF-CCSD/cc-pVDZ//MP2/cc-pVTZ. [b]Determined using structures that were stationary points at MP2/cc-pVTZ. [c]Determined using the SF energies to identify stationary points based on PES curvature. [d]Energies calculated at MP2/cc-pVTZ.

around **3a−d** and **7a−d** observed in the high-spin triplet reference calculations. Rather, we hypothesize that the documented[41] orbital instability of *ab initio* calculations of *para*-benzyne (arising from the near-degeneracy of electronic states of different symmetry) is extended to the similar structures that occur in the region around **3a−d** and **7a−d**, for both CCSD and DFT high-spin reference calculations. The difference between the solutions to these high-spin reference calculations appears to be related to the ordering of two radical-type orbitals associated with the *para*-benzyne structure and two π-type orbitals of the fused ring π system. This variation was corrected by adjusting the orbital guess for the reference calculation to obtain a continuous reference energy surface from the enediyne species (**2a−d** and **6a−d**) to the ring-opened species (**4a−d** and **8a−d**). The adjustment provided a continuous surface from the reactant to the product along the IRC, but the resultant energy values were not necessarily the lowest energy result for every electronic state for each structure in the reaction pathway.

RESULTS AND DISCUSSION

The computational results of the [2 + 2] and [4 + 2] carbon condensation reaction pathways investigated in this work are displayed in Figures 1 and 2, respectively, and summarized in Tables 1 and 2. Given the multiple ways in which the condensation of polyynes can proceed through the [2 + 2] and [4 + 2] cycloadditions, as discussed above, we did not pursue a comprehensive examination of the transformation from **1a−d** to **2a−d** and **1/5a−d** to **6a−d**. Instead, we directed our attention to the nature of the diradical species **3a−d** and **7a−d**, focusing on the transformations from **2a−d** to **3a−d** to **4a−d** and from **6a−d** to **7a−d** to **8a−d**. To this end, the reaction coordinate for Figure 1 is the combination of the IRC results for the transition states connecting **2a−d** and **3a−d** with the IRC results for the transition states connecting **3a−d** and **4a−d**. For several cases, the IRC calculations were unable to be extended all the way to the connected local minima within a reasonable amount of processor time. The local minima structures are therefore spaced between the IRC results in an energetically reasonable but ultimately arbitrary fashion. Similarly, Figure 2 is the combination of the IRC results for the transition states connecting **6a−d** and **7a−d** with the IRC

https://doi.org/10.1021/acs.jpca.3c00617
J. Phys. Chem. A 2023, 127, 4277−4290

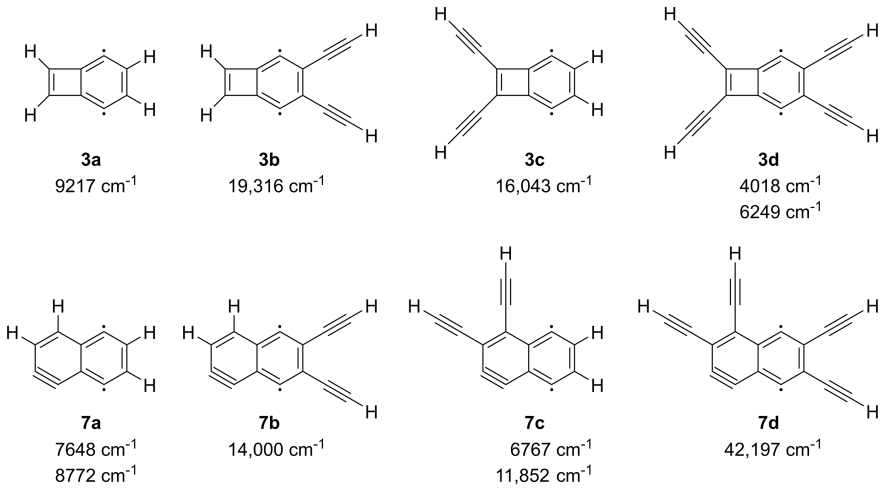

Figure 3. Species with unrealistically large harmonic vibrational frequencies as determined using MP2/cc-pVTZ calculations.

results for the transition states connecting **7a−d** and **8a−d**, with the local minima structures spaced between. For both figures, the reaction coordinate starts at the IRC calculated structure closest to the initial rings **2a−d** and **6a−d**. To connect the initial ring structures to the transition states *via* the IRC at the step size utilized would require an exceedingly long calculation due to the shallowness of the energy surface in this region.

The data depicted in Figures 1 and 2 and summarized in Tables 1 and 2 are reminiscent of those previously reported for the parent system **2a** → **3a** → **4a**.[21] The MP2 energies of the diradicals **3a−d** and **7a−d** are anomalously low relative to the spin-flip calculations, presumably because of the spin contamination problems that plague the application of MP2 in open-shell systems. Not only are the MP2 energies of diradicals **3** and **7** too low, the energies of the transition states leading to the diradicals are also too low. These problems affect the overall reaction thermochemistry and, in the case of diradicals **3a−d**, call into question whether these species even exist as local minima.

The reaction pathways detailed herein involve novel, highly unsaturated molecules, particularly that of the 1,2,5,8-tetradehydronaphthalene species **7a−d** that result from the Bergman cyclization of **6a−d** in the [4 + 2] pathway. While similar unsaturated naphthalene species have been previously studied computationally,[42] the current work is, to the best of our knowledge, the first to examine the 1,2,5,8 isomer **7a−d**. In Figures 1 and 2, zero-point vibrational energy (ZPVE) corrections were not included in the reported energies due to the unrealistically large vibrational frequencies calculated for the diradical species **3a−d** and **7a−d**. These frequencies (displayed in Figure 3) vary from 7000 to 42,000 cm^{-1} and significantly distort the ZPVE correction. A similar issue was previously observed in Hartree−Fock calculations of *para*-benzyne and was attributed to orbital instability effects in *para*-benzyne caused by the near-degeneracy of electronic configurations of different symmetry among the solutions to the HF equations.[41] This instability manifests in properties of the second-order and higher, such as vibrational frequencies, but in principle has no effect on the structure or its energy.[41] Considering that a *para*-benzyne moiety is present in each of the offending species, the observed orbital instability effects are likely the root cause of the abnormal frequencies.

Initial Cycloaddition. The initial cycloadditions for the model systems studied are considerably more exothermic for the [4 + 2] pathways **II** than the [2 + 2] pathways **I** (by 30 kcal/mol), which agrees with previous studies.[25,26] Such a result is expected as the [4 + 2] cycloaddition of **II** results in a strained, aromatic ring, whereas the [2 + 2] cycloaddition of **I** results in a strained, formally antiaromatic ring. The concerted transition states **TS1/5−6a** and **TS1/5−6c** that were located for the initial cycloadditions in **II** have a slightly lower activation barrier than those reported previously,[26,27,43] attributable to a difference in theory and basis set. There is a small variation in ΔE_{rxn} for the initial cycloaddition to form **2a−d**, and it appears that the inclusion of an alkynyl unit on the ring of **6** makes the initial cycloaddition producing **6c,d** less exothermic than **6a,b** (Table 2). The origin of this difference can be elucidated, to a degree, by comparing the reactions that form **6b** and **6c**, which share the same reactant alkynes (**1b** = **1c** and **5b** = **5c**). The computed energy difference (ΔE = 10.1 kcal/mol, Supporting Information) establishes that the initial cycloaddition favors the formation of the bis(diyne) **6b** over the tetrakis(mono-yne) **6c**. Our consideration of the NBO results for **6a**, **6b**, and **6c** did not reveal any obvious explanations for this energy difference, so to explore the origin of this energy difference, we computed the energy of cyclization for a variety of alkynyl substituted *ortho*-benzynes, as shown in Figure 4. A standard reference is required to eliminate the dependence of the energy of cyclization on different lengths of the initial polyynes. Thus, the cyclization energies have been calculated relative to acetylene (C_2H_2) and the polyyne (C_mH_2) necessary to obtain the molecular formula of the corresponding *ortho*-benzyne ($C_{m+2}H_4$). Given that the regioisomers of **6a** are all within 1 kcal/mol in energy of one another and that the linearity of the trend in Figure 4 demonstrates group additivity, we conclude that the difference in cyclization energy between **6a,b** and **6c,d** is a thermodynamic consequence of the number of alkynyl groups substituted on the *ortho*-benzyne ring (two and four, respectively). The substitution pattern or steric factors associated with the substitution pattern do not contribute significantly to the difference in cyclization energy.

Bergman Cyclization. Following the initial cyclization event—whether it is a [2 + 2] (**I**) or a [4 + 2] (**II**) reaction—the next step in the condensation pathway is proposed to be a

https://doi.org/10.1021/acs.jpca.3c00617
J. Phys. Chem. A 2023, 127, 4277−4290

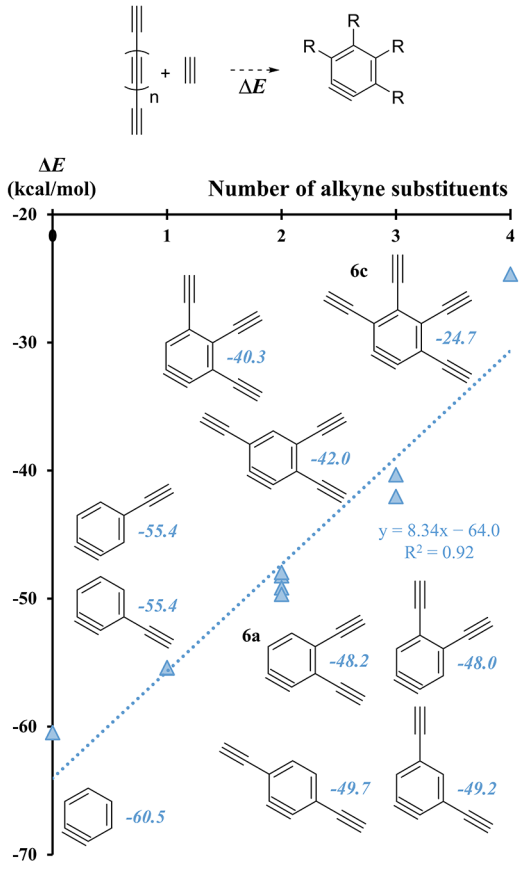

Figure 4. Reaction energies for formation of alkynyl-substituted *ortho*-benzynes, relative to acetylene and the appropriately mass-balanced polyyne (SF-TDDFT/cc-pVTZ//MP2/cc-pVTZ).

Bergman cycloaromatization reaction. The computed activation barriers for the cyclization step (**2** → **3** or **6** → **7**) vary significantly, depending on the computational method used (Table 2). This difference is directly attributable to the discrepancy in computed energy of the 1,4-didehydroarene (*para*-benzyne) intermediates **3** and **7** using SF-TDDFT or MP2 methodology. As described earlier, we do not consider the MP2 values to be reliable for a diradical intermediate of this type, so we focus on the SF-TDDFT values in our discussion. Consideration of the SF-TDDFT values reported in Table 2, the Bergman cyclization reaction in the [2 + 2] pathway (**2** → **3**) exhibits a higher barrier than that of the [4 + 2] pathway (**6** → **7**). This relationship is consistent with the fact that activation barriers for Bergman cyclizations have been strongly correlated to the distance separating the alkyne units,[44] with decreasing distance corresponding to decreasing activation barrier. As shown in Table 3, the average distances are 5.2 and 4.1 Å for **2** and **6**, respectively, and the average eneyne angle is 136° and 120° for **2** and **6**, respectively.

For both pathways **I** and **II**, substitution patterns **a** and **c** are less endothermic and, consequently, have lower activation barriers to Bergman cyclization. These cases afford cyclization products that do not bear alkyne substituents directly on the *para*-benzyne ring (**3a**, **3c**, **7a**, **7c**). In contrast, the substitution patterns that place alkyne substituents directly on the *para*-benzyne ring (**3b**, **3d**, **7b**, **7d**) are more endothermic and have higher activation energies for Bergman cyclization. Analysis of the NBO/NRT results for **3a**, **3b**, **7a**, and **7b** (Supporting Information) suggests that the alkynyl units destabilize the

Table 3. Geometric Parameters of Enediyne Moieties (MP2/cc-pVTZ)

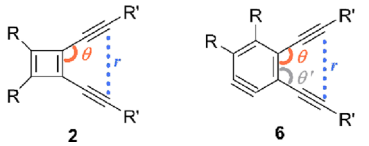

2 **6**

		r (Å)	*θ* (°)	*θ′* (°)
2	**a**	5.15	135.5	-
	b	5.14	135.2	-
	c	5.22	136.4	-
	d	5.23	136.3	-
	average	*5.18*	*135.9*	-
6	**a**	4.11	118.8	122.4
	b	4.03	118.2	121.8
	c	4.09	118.6	122.4
	d	4.02	118.3	121.7
	average	*4.06*	*118.5*	*122.1*

para-benzyne portion of the ring due to a decrease in the stabilization of the radical orbitals through hyperconjugation. Specifically, the overlap of the σ_{CH} and σ_{CH}* orbitals with the radical orbitals of the *para*-benzyne moiety in **3a** and **7a** provides stabilization *via* hyperconjugation (8.6 and 9.2 kcal/mol, respectively) that is nearly twice the stabilization from the overlap of the σ_{CC} and σ_{CC}* orbitals with the radical orbitals in **3b** and **7b** (5.0 and 4.9 kcal/mol, respectively). While it is possible that steric repulsions between the *ortho*-substituted alkyne units could be responsible for the destabilization of the *para*-benzyne moiety, this is contradicted by the reaction energy trends shown in Figure 5, which illustrates a linear change in the reaction energy of the Bergman cyclizations of **2** and **6** as alkyne units are substituted to the ring. Thus, we conclude that any steric interactions due to adjacent alkynyl units have very little impact on the energy of the molecule, which is consistent with the narrow steric profile of alkynyl substituents.

Before continuing the rest of the analysis, we note that an alternate Bergman cyclization is possible for **6c** and **6d** instead of that represented by **TS6−7c** and **TS6−7d**. In the alternate case, the alkyne units directly opposite the triple bond of the *ortho*-benzyne ring of **6** undergo the Bergman cyclization to yield a substituted 2,3,5,8-tetradehydronaphthalene species analogous to **7**. Our preliminary investigation of this alternate pathway is summarized in the Supporting Information, and the results indicate that this alternate pathway is similar or higher in energy. Most importantly, a large barrier inhibits the ring expansion reaction of the tetradehydronaphthalene species. Therefore, our conclusion—that pathway **II** forms a stable, fused *para*-benzyne ring which can continue to react as part of the ring coalescence and annealing model (*vide infra*)—remains the same. Fully exploring the competition of the alkyne substituents of *ortho*-benzyne to undergo Bergman cyclization requires large model systems, which is beyond the scope of this work and at the limits of current computing power. This may be something that can be addressed in future studies exploring carbon condensation reactions and the ring coalescence and annealing model.

Ring Expansion (Retro-Bergman Cyclization). The ring expansion (*via* a retro-Bergman cyclization mechanism) of **3a−d** to **4a−d** occurs virtually without a barrier (Figure 1). As described previously for the overall conversion of enediyne **2a** to cyclooctadienediyne **4a**,[21] there is a substantial energy

https://doi.org/10.1021/acs.jpca.3c00617
J. Phys. Chem. A 2023, 127, 4277−4290

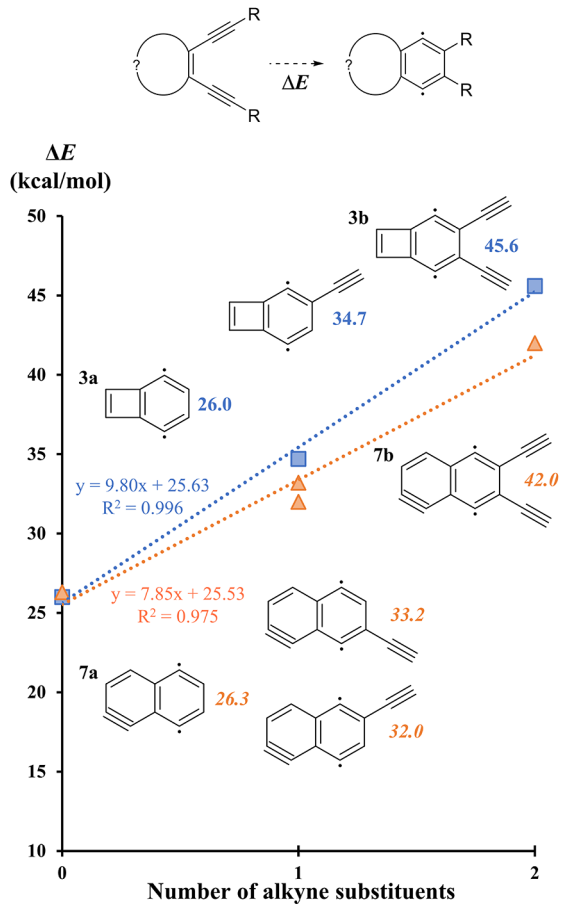

Figure 5. Reaction energies for the Bergman cyclizations of alkynyl-substituted cyclobutadienes (blue) and *ortho*-benzynes (orange) that form *para*-benzyne moieties (SF-TDDFT/cc-pVTZ//MP2/cc-pVTZ).

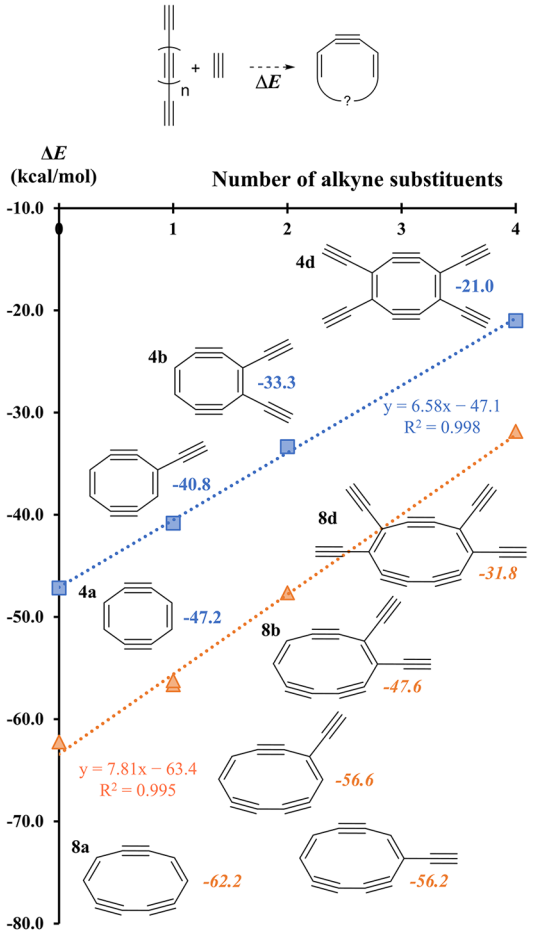

Figure 6. Reaction energies for the formation of substituted ring expansion products cyclooctadienediyne (blue) and cyclodecadiene-triyne (orange), relative to acetylene and the appropriately mass-balanced polyyne (SF-TDDFT/cc-pVTZ//MP2/cc-pVTZ).

change of 70−90 kcal/mol from the top of the highest barrier (**TS2−3**) to the product (**4**). This large energy change makes it difficult, topologically, for diradical **3** to exist as a minimum on the potential energy surface or for there to be a transition state barrier to ring opening to cyclooctadienediyne **4**. This contrasts with the ring expansions of **7a−d** to **8a−d**, which have activation barriers of 8−9 kcal/mol and corresponding energy changes (**TS6−7** to **8**) that are not as dramatically large (*ca.* 60 kcal/mol).

To gain insight into the energy changes associated with substitution of the ring-opened products **4a−d** and **8a−d**, we computed the energies of the ring-opened products relative to acetylene (C_2H_2) and the polyyne (C_mH_2) necessary to obtain the molecular formula of the corresponding product (**4** or **8**) (Figure 6). The linearity of the trends in Figure 6 demonstrates group additivity, which excludes the involvement of steric interactions among the substituents. Furthermore, in the case of cyclodecadienetriyne derivatives (**8**), the regioisomeric monosubstituted compounds are within 0.3 kcal/mol in energy of one another. The substitution pattern or steric factors associated with the substitution pattern do not contribute to the difference in cyclization energy. We therefore conclude that the difference in cyclization energy of **4a−d** and **8a−d** is a thermodynamic consequence of the differences in the number of substituents.

Reaction Pathways I and II. Consistent with the analyses associated with Figures 4 and 6, particularly that the alkyne substituents have little interaction with other alkyne substituents, is the fact that the reaction energetics for substitution pattern **d** can be predicted empirically using the reaction energetics of cases **a−c**. The **d** substitution pattern has alkyne units substituted on the *para*-benzyne ring and on the initially formed ring (cyclobutadiene in **I**, *ortho*-benzyne in **II**), while the **a** substitution pattern is the parent, unsubstituted system (R = R′ = H). To understand the difference in energy between the structures in **d** compared to those in **a**, we must account for three effects: the energetic impact of replacing hydrogens with alkyne units on the *para*-benzyne ring, the energetic impact of replacing hydrogens with alkyne units on the initially formed ring, and the interaction between the substituents when both rings are substituted with alkyne units. The first effect is accounted for by the difference between **b** and **a**, while the second effect is accounted for by the difference between **c** and **a**. We could attempt to account for the third effect by considering additional substitution patterns, but it is apparent from Table 4 that this effect is small in magnitude since the difference between **d** and **a** can be predicted to ±2 kcal/mol (SF-TDDFT/cc-pVTZ//MP2/cc-pVTZ) using only the first two effects.

https://doi.org/10.1021/acs.jpca.3c00617
J. Phys. Chem. A 2023, 127, 4277−4290

Table 4. Empirical Demonstration of Independent Substituent Effect (kcal/mol)

			initial cycloaddition (1−2 and 1/5−6)		Bergman cyclization (2−3 and 6−7)		ring expansion (3−4 and 7−8)	
			$\Delta E^{\ddagger}$	ΔE_{rxn}	$\Delta E^{\ddagger}$	ΔE_{rxn}	$\Delta E^{\ddagger}$	ΔE_{rxn}
MP2	I	**d** − **a**		−1.0	1.8	−15.9	2.6	−4.9
		(**b** − **a**) + (**c** − **a**)		−1.9	0.9	−15.0	2.6	−4.7
		difference		−0.9	−0.9	−0.9	0.0	−0.2
	II	**d** − **a**		12.5	3.9	11.8	2.1	0.0
		(**b** − **a**) + (**c** − **a**)		12.0	3.6	11.3	2.1	−0.1
		difference		−0.5	−0.3	−0.5	0.0	−0.1
SF-TDDFT	I	**d** − **a**		0.6	15.6	22.6		1.1
		(**b** − **a**) + (**c** − **a**)		−1.3	15.9	24.7		0.9
		difference		−1.9	0.3	2.1		−0.2
	II	**d** − **a**		15.4	11.1	15.4	1.4	−0.8
		(**b** − **a**) + (**c** − **a**)		14.6	10.9	16.4	0.2	−1.9
		difference		−0.8	−0.2	1.0	−1.2	−1.1

An interesting feature of these reactions is that after the initial cycloaddition of the polyynes, the reactions being investigated involve no formal change in aromaticity. In pathway **I**, **2** is a 4-electron cyclic π system and both **3** and **4** are 8-electron cyclic π systems; thus, **2**, **3**, and **4** are formally antiaromatic. In pathway **II**, **6** is a 6-electron cyclic π system and both **7** and **8** are 10-electron cyclic π systems; thus, **6**, **7**, and **8** are formally aromatic. To assess the degree of aromaticity (or antiaromaticity) in the species studied, NICS values[36] have been calculated at B3LYP/6-31G(d) using the MP2/cc-pVTZ optimized structures. We report $NICS_{zz}(1)$ values in Table 5 using the NMR convention where positive values correspond to antiaromatic character and negative values correspond to aromatic character. The $NICS_{zz}(1)$ values, which have been shown to be effective measures of aromaticity,[45] were obtained by taking the *zz* component (the direction perpendicular to the ring) of the magnetic shielding tensor of a ghost atom placed 1 Å above and perpendicular to the center of the ring. In the case of bicyclic structures **3** and **7**, we report the $NICS_{zz}(1)$ values for the center of each of the fused rings. The results given in Table 5 confirm that **6**, **7**, and **8** have a significant aromatic character and that **2** and **4** have a significant antiaromatic character. The $NICS_{zz}(1)$ values for **3** taken at the center of the cyclobutadiene ring and the center of the *para*-benzyne ring indicate antiaromatic and aromatic character, respectively. All species show that substitution of alkyne units decreases the magnitude of the $NICS_{zz}(1)$ values, *i.e.*, the values move closer to zero. The results in Table 5 show a qualitative agreement with previous studies involving molecules from this work (**2a**,[46] **2c**,[46] **3a**,[36,47] and **4a**[47]) as well as in comparison to similar species (cyclobutadiene,[46,48] *ortho*-benzyne,[49] *para*-benzyne,[49] and naphthalene[36]). We attribute the quantitative differences to the choice of computational methodology and basis sets for the structure optimizations and subsequent NICS calculations.

Table 5. Nucleus-Independent Chemical Shift [$NICS_{zz}(1)$] Values of Molecules in Pathways I and II

	center of ring	center of original ring	center of *para*-benzyne ring	center of ring
I	**2**		**3**	**4**
a	14.8	18.8	−9.5	22.1
b	13.8	17.1	−8.9	19.9
c	11.5	15.8	−10.6	19.9
d	11.0	14.3	−9.9	18.1
II	**6**		**7**	**8**
a	−13.5	−12.4	−21.7	−13.9
b	−12.2	−11.6	−21.4	−12.6
c	−11.6	−11.0	−21.1	−12.6
d	−11.3	−10.1	−21.4	−11.4

We can now provide a general explanation of the relative stabilities and reaction energies of the [2 + 2] (**I**) and [4 + 2] (**II**) pathways for the condensation of polyynes. The initial cycloaddition to form cyclobutadiene **2** or *ortho*-benzyne **6** is governed by the ring strain and degree of (anti)aromatic character. Therefore, formation of **2** (a highly strained and antiaromatic ring) is less exothermic than the formation of **6** (a partially strained and aromatic ring). Bergman cyclization of the alkyne substituents to form a *para*-benzyne ring is endothermic. The activation barriers for the Bergman cyclization of **2** and **6** are in accord with qualitative expectations based upon the distance between terminal carbons of the alkyne substituents. The subsequent ring expansion removes the diradical character and relieves the ring strain and thus is exothermic. The opening of the fused rings has a greater impact on the stability of the structure in **I** compared to that in **II**: the transformation from **3** to **4** has effectively no activation barrier and is more exothermic than the transformation from **6** to **7**, which does have an activation barrier. Substitution of alkyne units to the ring structures in **I** and **II** is destabilizing—due to the decrease in hyperconjugation strength caused by the replacement of hydrogen atoms with more electronegative sp-hybridized carbon atoms of the alkyne units[50]—but has little effect on the energetics of the retro-Bergman cyclization.

The Medium Rings. The current investigation draws attention to highly unsaturated cyclooctane and cyclodecane derivatives—medium ring compounds that are not commonly invoked in carbon condensation processes. Whether derivatives of cyclooctadienediyne **4** or cyclodecadienetriyne **8** might be directly involved in reaction pathways for carbon condensation or whether they are simply reservoirs of carbon generated under harsh reaction conditions is a topic for further investigation. It is not inconceivable that medium ring intermediates could lead to carbon condensation (Scheme 5). One mode of cyclization of a cyclooctane derivative may generate a bicyclo[3.3.0]octane structure, which consists of fused 5-membered rings. Although fullerenes do not contain

https://doi.org/10.1021/acs.jpca.3c00617
J. Phys. Chem. A 2023, 127, 4277−4290

Scheme 5. Reaction Pathways Involving Collapse of Medium Rings

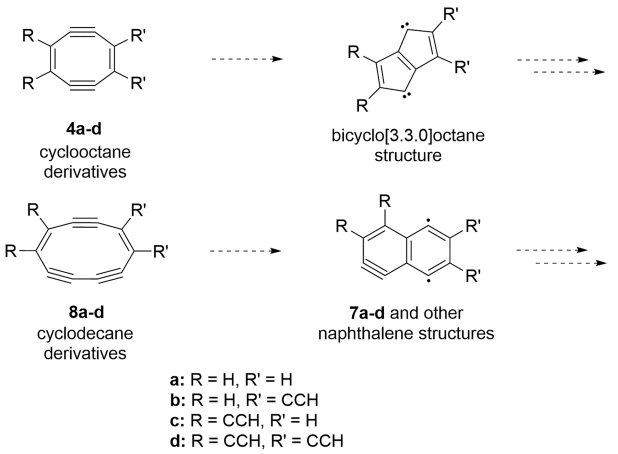

fused 5-membered rings (the 'isolated pentagon rule'),[20,51,52] the Stone–Wales rearrangement or other rearrangement reactions allow 5-membered rings to migrate in a sheet of carbon.[52,53] In the current study, the cyclodecane skeleton was derived from a dehydronaphthalene precursor (Scheme 4). Depending on the nature of substituents and substitution pattern, a cyclodecane derivative may afford the possibility for structural rearrangement and to permute the substituents on a dehydronaphthalene skeleton. The structures depicted in Scheme 5 are representative of carbon connectivity and not representative of the degree of hydrogenation, nature of substituents, or details of reaction mechanisms (thermal, radical-catalyzed, *etc.*).

CONCLUSIONS

The *para*-benzyne intermediate in **I** (produced by the Bergman cyclization of the product of a [2 + 2] cycloaddition of two polyynes) is much more likely to undergo a ring expansion (*via* a retro-Bergman cyclization mechanism) than the corresponding *para*-benzyne intermediate in **II** (produced similarly to **I** but with an initial [4 + 2] cycloaddition), with activation barriers differing by roughly a factor of two according to MP2 calculations. With the results of the spin-flip calculations, we may extend this conclusion even further to say that the *para*-benzyne intermediate **I** is not even a stationary point on the potential energy surface. According to the same spin-flip calculations, however, the *para*-benzyne intermediate **II** is a stationary point with an activation barrier of 8–10 kcal/mol to undergo the ring expansion.

We previously proposed[21] that the activation barrier for the ring expansion of **3a** to **4a** is small due to the large exothermicity of the reaction of **2a** to **4a**. This argument is not sufficient to explain the difference in activation barriers between **I** and **II** as determined using the spin-flip methods. As seen in Table 1, the transformation from **2** to **4** is exothermic by 11–35 kcal/mol, while the corresponding transformation from **6** to **8** is exothermic by 3–18 kcal/mol; yet, the activation barriers for the ring expansions in **I** are clearly distinct from those in **II**. It appears, rather, that the exothermicity of the ring expansion itself is responsible for the activation barriers. The ring expansions in **I** are exothermic by 55–66 kcal/mol and have effectively no activation barriers, while the ring expansions in **II** are exothermic by 44–46 kcal/mol and have activation barriers of 8–10 kcal/mol. The reason for the larger exothermicity for the ring expansion in **I** most certainly lies in the removal of the highly strained cyclobutadiene moiety. This stabilizing driving force to undergo the ring expansion is missing from the corresponding transformation in **II**.

Extension and improvement of the analysis herein is hampered by computational limitations of the methods employed. Examination of how increasing the length of the initial polyynes, *i.e.*, extending the possible substitutions of R and R′ in Scheme 4 to include CCCCH, affects the systems in question requires prohibitively long calculations, as does calculating EOM-SF-CCSD energies for the structures with substitution patterns **b**–**d**. Optimizations of the *para*-benzyne intermediates and transition states using SF-TDDFT were plagued by the orbital instability of the *para*-benzyne moiety in the high-spin reference calculations, similar to what we encountered for the single-point calculations. Despite the limitations of this work, however, the consistency of reaction energetics of the ring expansion in **I** and **II** suggests that further incorporation of alkyne units will have little effect on the likelihood of the *para*-benzyne intermediate undergoing a ring expansion. We therefore maintain that formation of fullerene *via* the ring coalescence and annealing model likely proceeds through an initial [4 + 2] cycloaddition rather than a [2 + 2] cycloaddition.

ASSOCIATED CONTENT

Supporting Information

The Supporting Information is available free of charge at https://pubs.acs.org/doi/10.1021/acs.jpca.3c00617.

Select NBO orbitals and hyperconjugation analysis; MP2/cc-pVTZ geometric parameters of molecules in pathways **I** and **II**; MP2/cc-pVTZ computational data: stationary point data overview; directory of stationary point data; energies and Cartesian coordinates (PDF)

AUTHOR INFORMATION

Corresponding Author

Robert J. McMahon – *Department of Chemistry, University of Wisconsin-Madison, Madison, Wisconsin 53706, United States;* orcid.org/0000-0003-1377-5107; Email: robert.mcmahon@wisc.edu

Authors

Andrew N. Owen – *Department of Chemistry, University of Wisconsin-Madison, Madison, Wisconsin 53706, United States;* orcid.org/0000-0001-5903-1651

Brian J. Esselman – *Department of Chemistry, University of Wisconsin-Madison, Madison, Wisconsin 53706, United States;* orcid.org/0000-0002-9385-8078

R. Claude Woods – *Department of Chemistry, University of Wisconsin-Madison, Madison, Wisconsin 53706, United States;* orcid.org/0000-0003-0865-4693

Complete contact information is available at: https://pubs.acs.org/10.1021/acs.jpca.3c00617

Notes

The authors declare no competing financial interest.

https://doi.org/10.1021/acs.jpca.3c00617
J. Phys. Chem. A 2023, 127, 4277–4290

■ ACKNOWLEDGMENTS

We thank the late Professor Hans J. Reich for providing the initial inspiration to examine the implications of the [4 + 2] cycloaddition. We also thank Andrew J. Wiederhold and Desiree M. Bates for conducting preliminary calculations. We gratefully acknowledge the National Science Foundation for support of this project (CHE-1664912 and CHE-1954270).

■ REFERENCES

(1) Hou, L.; Cui, X.; Guan, B.; Wang, S.; Li, R.; Liu, Y.; Zhu, D.; Zheng, J. Synthesis of a monolayer fullerene network. *Nature* **2022**, *606*, 507.
(2) Chen, Z.; Narita, A.; Müllen, K. Graphene Nanoribbons: On-Surface Synthesis and Integration into Electronic Devices. *Adv. Mater.* **2020**, *32*, 2001893.
(3) Fan, Q.; Yan, L.; Tripp, M. W.; Krejčí, O.; Dimosthenous, S.; Kachel, S. R.; Chen, M.; Foster, A. S.; Koert, U.; Liljeroth, P.; et al. Biphenylene network: A nonbenzenoid carbon allotrope. *Science* **2021**, *372*, 852−856.
(4) Diederich, F.; Rubin, Y.; Knobler, C. B.; Whetten, R. L.; Schriver, K. E.; Houk, K. N.; Li, Y. All-Carbon Molecules: Evidence for the Generation of Cyclo[18]carbon from a Stable Organic Precursor. *Science* **1989**, *245*, 1088−1090.
(5) Anderson, H. L.; Patrick, C. W.; Scriven, L. M.; Woltering, S. L. A Short History of Cyclocarbons. *Bull. Chem. Soc. Jpn.* **2021**, *94*, 798−811.
(6) McElvany, S. W.; Ross, M. M.; Goroff, N. S.; Diederich, F. Cyclocarbon Coalescence: Mechanisms for Tailor-Made Fullerene Formation. *Science* **1993**, *259*, 1594−1596.
(7) Kaiser, K.; Scriven, L. M.; Schulz, F.; Gawel, P.; Gross, L.; Anderson, H. L. An sp-hybridized molecular carbon allotrope, cyclo[18]carbon. *Science* **2019**, *365*, 1299−1301. see Erratum 13 March 2020.
(8) Chuvilin, A.; Kaiser, U.; Bichoutskaia, E.; Besley, N. A.; Khlobystov, A. N. Direct transformation of graphene to fullerene. *Nat. Chem.* **2010**, *2*, 450−453.
(9) Thakur, A. K.; Muralidharan, K.; Zega, T. J.; Ziurys, L. M. A nanometric window on fullerene formation in the interstellar medium: Insights from molecular dynamics studies. *J. Chem. Phys.* **2022**, *156*, 154704.
(10) Pietrucci, F.; Andreoni, W. Fate of a Graphene Flake: A New Route toward Fullerenes Disclosed with Ab Initio Simulations. *J. Chem. Theor. Comput.* **2014**, *10*, 913−917.
(11) Neng, W.; Shuang-ying, L.; Jun, X.; Matteo, M.; Yi-long, Z.; Shu, W.; Li-tao, S.; Qing-an, H. Fullerene growth from encapsulated graphene flakes. *Nanoscale* **2014**, *6*, 11213−11218.
(12) Irle, S.; Zheng, G.; Wang, Z.; Morokuma, K. The C_{60} Formation Puzzle "Solved:" QM/MD Simulations Reveal the Shrinking Hot Giant Road of the Dynamic Fullerene Self-Assembly Mechanism. *J. Phys. Chem. B* **2006**, *110*, 14531−14545.
(13) Huang, J. Y.; Ding, F.; Jiao, K.; Yakobson, B. I. Real Time Microscopy, Kinetics, and Mechanism of Giant Fullerene Evaporation. *Phys. Rev. Lett.* **2007**, *99*, No. 175503.
(14) Heath, J. R. Synthesis of C_{60} from Small Carbon Clusters: A Model Based on Experiment and Theory. In *Fullerenes: Synthesis, Properties, and Chemistry of Large Carbon Clusters*; Hammond, G. S.; Kuck, V. J. Eds.; American Chemical Society: Washington, DC, 1992; Vol. *481*, pp. 1−23.
(15) Smalley, R. E. Self-assembly of the fullerenes. *Acc. Chem. Res.* **1992**, *25*, 98−105.
(16) Dunk, P. W.; Kaiser, N. K.; Hendrickson, C. L.; Quinn, J. P.; Ewels, C. P.; Nakanishi, Y.; Sasaki, Y.; Shinohara, H.; Marshall, A. G.; Kroto, H. W. Closed network growth of fullerenes. *Nat. Commun.* **2012**, *3*, 855.
(17) Dunk, P. W.; Mulet-Gas, M.; Rodríguez-Fortea, A.; Poblet, J. M.; Marshall, A. G.; Kroto, H. W. Recent advances in fullerene science. *AIP Conf. Proc.* **2014**, *1628*, 862−869.
(18) Rubin, Y.; Kahr, M.; Knobler, C. B.; Diederich, F.; Wilkins, C. L. The higher oxides of carbon $C_{8n}O_{2n}$ (n = 3-5): synthesis, characterization, and x-ray crystal structure. Formation of cyclo[n] carbon ions C_n^+ (n = 18, 24), C_n^- (n = 18, 24, 30), and higher carbon ions including C_{60}^+ in laser desorption Fourier transform mass spectrometric experiments. *J. Am. Chem. Soc.* **1991**, *113*, 495−500.
(19) Hunter, J. M.; Fye, J. L.; Roskamp, E. J.; Jarrold, M. F. Annealing Carbon Cluster Ions: A Mechanism for Fullerene Synthesis. *J. Phys. Chem.* **1994**, *98*, 1810−1818.
(20) Goroff, N. S. Mechanism of fullerene formation. *Acc. Chem. Res.* **1996**, *29*, 77−83.
(21) Esselman, B. J.; Emmert, F. L., III; Wiederhold, A. J.; Thompson, S. J.; Slipchenko, L. V.; McMahon, R. J. Thermal Isomerizations of Diethynyl Cyclobutadienes and Implications for Fullerene Formation. *J. Org. Chem.* **2015**, *80*, 11863−11868.
(22) Hoye, T. R.; Baire, B.; Niu, D.; Willoughby, P. H.; Woods, B. P. The hexadehydro-Diels−Alder reaction. *Nature* **2012**, *490*, 208−212.
(23) Holden, C.; Greaney, M. F. The Hexadehydro-Diels−Alder Reaction: A New Chapter in Aryne Chemistry. *Angew. Chem., Int. Ed.* **2014**, *53*, 5746−5749.
(24) Cremer, D.; Kraka, E.; Joo, H.; Stearns, J. A.; Zwier, T. S. Exploration of the potential energy surface of C_4H_4 for rearrangement and decomposition reactions of vinylacetylene: A computational study. Part I. *Phys. Chem. Chem. Phys.* **2006**, *8*, 5304−5316.
(25) Cahill, K. J.; Ajaz, A.; Johnson, R. P. New Thermal Routes to *ortho*-Benzyne. *Aust. J. Chem.* **2010**, *63*, 1007−1012.
(26) Ajaz, A.; Bradley, A. Z.; Burrell, R. C.; Li, W. H. H.; Daoust, K. J.; Bovee, L. B.; DiRico, K. J.; Johnson, R. P. Concerted vs Stepwise Mechanisms in Dehydro-Diels−Alder Reactions. *J. Org. Chem.* **2011**, *76*, 9320−9328.
(27) Ghigo, G.; Maranzana, A.; Tonachini, G. *o*-Benzyne fragmentation and isomerization pathways: a CASPT2 study. *Phys. Chem. Chem. Phys.* **2014**, *16*, 23944−23951.
(28) Liang, Y.; Hong, X.; Yu, P.; Houk, K. N. Why Alkynyl Substituents Dramatically Accelerate Hexadehydro-Diels−Alder (HDDA) Reactions: Stepwise Mechanisms of HDDA Cycloadditions. *Org. Lett.* **2014**, *16*, 5702−5705.
(29) Jones, R. R.; Bergman, R. G. *p*-Benzyne. Generation as an intermediate in a thermal isomerization reaction and trapping evidence for the 1,4-benzenediyl structure. *J. Am. Chem. Soc.* **1972**, *94*, 660−661.
(30) Shao, Y.; Head-Gordon, M.; Krylov, A. I. The spin−flip approach within time-dependent density functional theory: Theory and applications to diradicals. *J. Chem. Phys.* **2003**, *118*, 4807−4818.
(31) Bernard, Y. A.; Shao, Y.; Krylov, A. I. General formulation of spin-flip time-dependent density functional theory using non-collinear kernels: Theory, implementation, and benchmarks. *J. Chem. Phys.* **2012**, *136*, 204103.
(32) Møller, C.; Plesset, M. S. Note on an Approximation Treatment for Many-Electron Systems. *Phys. Rev.* **1934**, *46*, 618−622.
(33) Dunning, T. H., Jr. Gaussian-Basis Sets for use in Correlated Molecular Calculations. I. The Atoms Boron through Neon and Hydrogen. *J. Chem. Phys.* **1989**, *90*, 1007−1023.
(34) Frisch, M. J.; Trucks, G. W.; Schlegel, H. B.; Scuseria, G. E.; Robb, M. A.; Cheeseman, J. R.; Scalmani, G.; Barone, V.; Mennucci, B.; Petersson, G. A. et al. *Gaussian 09, Revision D.01*; Gaussian, Inc.: Wallingford, CT, USA, 2009.
(35) Shao, Y.; Gan, Z.; Epifanovsky, E.; Gilbert, A. T. B.; Wormit, M.; Kussmann, J.; Lange, A. W.; Behn, A.; Deng, J.; Feng, X.; et al. Advances in molecular quantum chemistry contained in the Q-Chem 4 program package. *Mol. Phys.* **2015**, *113*, 184−215.
(36) Chen, Z.; Wannere, C. S.; Corminboeuf, C.; Puchta, R.; Schleyer, P. v. R. Nucleus-Independent Chemical Shifts (NICS) as an Aromaticity Criterion. *Chem. Rev.* **2005**, *105*, 3842−3888.
(37) Glendening, E. D.; Badenhoop, J. K.; Reed, A. E.; Carpenter, J. E.; Bohmann, J. A.; Morales, C. M.; Landis, C. R.; Weinhold, F. *NBO 6.0*; Theoretical Chemistry Institute, University of Wisconsin: Madison, WI, 2013.

https://doi.org/10.1021/acs.jpca.3c00617
J. Phys. Chem. A 2023, 127, 4277−4290

(38) Lee, C.; Yang, W.; Parr, R. G. Development of the Colle-Salvetti Correlation-Energy Formula into a Functional of the Electron-Density. *Phys. Rev. B* **1988**, *37*, 785−789.
(39) Becke, A. D. Density-Functional Thermochemistry. III. The Role of Exact Exchange. *J. Chem. Phys.* **1993**, *98*, 5648−5652.
(40) Hehre, W. J.; Ditchfield, R.; Pople, J. A. Self-Consistent Molecular Orbital Methods. XII. Further Extensions of Gaussian-Type Basis Sets for Use in Molecular Orbital Studies of Organic Molecules. *J. Chem. Phys.* **1972**, *56*, 2257−2261.
(41) Crawford, T. D.; Kraka, E.; Stanton, J. F.; Cremer, D. Problematic *p*-benzyne: Orbital instabilities, biradical character, and broken symmetry. *J. Chem. Phys.* **2001**, *114*, 10638−10650.
(42) Pauzat, F.; Talbi, D.; Ellinger, Y. UIR bands: Computational experiments on the IR spectra of naphthalene derivatives as models for PAHs. *Astron. Astrophys.* **1995**, *293*, 263−277.
(43) Zhang, X.; Maccarone, A. T.; Nimlos, M. R.; Kato, S.; Bierbaum, V. M.; Ellison, G. B.; Ruscic, B.; Simmonett, A. C.; Allen, W. D.; Schaefer, H. F. Unimolecular thermal fragmentation of *ortho*-benzyne. *J. Chem. Phys.* **2007**, *126*, 044312.
(44) Mohamed, R. K.; Peterson, P. W.; Alabugin, I. V. Concerted Reactions That Produce Diradicals and Zwitterions: Electronic, Steric, Conformational, and Kinetic Control of Cycloaromatization Processes. *Chem. Rev.* **2013**, *113*, 7089−7129.
(45) Fallah-Bagher-Shaidaei, H.; Wannere, C. S.; Corminboeuf, C.; Puchta, R.; Schleyer, P. v. R. Which NICS Aromaticity Index for Planar π Rings Is Best? *Org. Lett.* **2006**, *8*, 863−866.
(46) Esselman, B. J.; McMahon, R. J. Effects of ethynyl substitution on cyclobutadiene. *J. Phys. Chem. A* **2012**, *116*, 483−490.
(47) Tsipis, A. C. Efficiency of the $NICS_{zz}$-scan curves to probe the antiaromaticity of organic and inorganic rings/cages. *Phys. Chem. Chem. Phys.* **2009**, *11*, 8244−8261.
(48) Schleyer, P. v. R.; Manoharan, M.; Wang, Z.-X.; Kiran, B.; Jiao, H.; Puchta, R.; van Eikema Hommes, N. J. R. Dissected Nucleus-Independent Chemical Shift Analysis of π-Aromaticity and Antiaromaticity. *Org. Lett.* **2001**, *3*, 2465−2468.
(49) De Proft, F.; von Ragué Schleyer, P.; van Lenthe, J. H.; Stahl, F.; Geerlings, P. Magnetic Properties and Aromaticity of *o*-, *m*-, and *p*-Benzyne. *Chem. − Eur. J.* **2002**, *8*, 3402−3410.
(50) Alabugin, I. V.; dos Passos Gomes, G.; Abdo, M. A. Hyperconjugation. *Wiley Interdiscip. Rev.: Comput. Mol. Sci.* **2019**, *9*, e1389.
(51) Mintmire, J. W. Fullerene Formation and Annealing. *Science* **1996**, *272*, 45−46.
(52) Mitchell, I.; Qiu, L.; Lamb, L. D.; Ding, F. High Temperature Accelerated Stone−Wales Transformation and the Threshold Temperature of IPR-C_{60} Formation. *J. Phys. Chem. A* **2021**, *125*, 4548−4557.
(53) Irace, E. E.; Brayfindley, E.; Vinnacombe, G. A.; Castro, C.; Karney, W. L. Stone−Wales Rearrangements in Hydrocarbons: From Planar to Bowl-Shaped Substrates. *J. Org. Chem.* **2015**, *80*, 11718−11725.

https://doi.org/10.1021/acs.jpca.3c00617
J. Phys. Chem. A 2023, 127, 4277−4290